



Available online at www.sciencedirect.com

ScienceDirect

www.elsevier.com/locate/jes

JES
JOURNAL OF
ENVIRONMENTAL
SCIENCES
www.jesc.ac.cn

Chemical formation and source apportionment of PM_{2.5} at an urban site at the southern foot of the Taihang mountains

Xiaoyong Liu^{1,2,8}, Mingshi Wang³, Xiaole Pan^{2,*}, Xiyue Wang^{4,*},
Xiaolong Yue⁵, Donghui Zhang⁴, Zhigang Ma⁵, Yu Tian^{2,8}, Hang Liu^{2,8},
Shandong Lei^{2,8}, Yuting Zhang^{2,8}, Qi Liao^{2,8}, Baozhu Ge², Dawei Wang²,
Jie Li², Yele Sun², Pingqing Fu⁷, Zifa Wang^{1,2,9}, Hong He^{1,6}

¹ Center for Excellence in Regional Atmospheric Environment, Institute of Urban Environment, Chinese Academy of Sciences, Xiamen 361021, China

² State Key Laboratory of Atmospheric Boundary Layer Physics and Atmospheric Chemistry, Institute of Atmospheric Physics, Chinese Academy of Sciences, Beijing 100029, China

³ Henan Polytechnic University, Jiaozuo 454003, China

⁴ Jiaozuo Ecological Environment Monitoring Center, Jiaozuo 454003, China

⁵ Jiaozuo Environmental Science Research Institute, Jiaozuo 454003, China

⁶ Research Center for Eco-Environmental Sciences, Chinese Academy of Sciences, Beijing 100085, China

⁷ Institute of Surface-Earth System Science, Tianjin University, Tianjin 300072, China

⁸ University of Chinese Academy of Sciences, Beijing 100049, China

⁹ College of Earth Sciences, University of Chinese Academy of Sciences, Beijing 100049, China

ARTICLE INFO

Article history:

Received 8 June 2020

Revised 30 September 2020

Accepted 6 October 2020

Available online 24 October 2020

ABSTRACT

The region along the Taihang Mountains in the North China Plain (NCP) is characterized by serious fine particle pollution. To clarify the formation mechanism and controlling factors, an observational study was conducted to investigate the physical and chemical properties of the fine particulate matter in Jiaozuo city, China. Mass concentrations of the water-soluble ions (WSIs) in PM_{2.5} and gaseous pollutant precursors were measured on an hourly basis from December 1, 2017, to February 27, 2018. The positive matrix factorization (PMF) method and the FLEXible PARTICle (FLEXPART) model were employed to identify the sources of PM_{2.5}. The results showed that the average mass concentration of PM_{2.5} was 111 μg/m³ during the observation period. Among the major WSIs, sulfate, nitrate, and ammonium (SNA) constituted 62% of the total PM_{2.5} mass, and NO₃⁻ ranked the highest with an average contribution of 24.6%. NH₄⁺ was abundant in most cases in Jiaozuo. According to chemical balance analysis, SO₄²⁻, NO₃⁻, and Cl⁻ might be present in the form of (NH₄)₂SO₄, NH₄NO₃, NH₄Cl, and KCl. The liquid-phase oxidation of SO₂ and NO₂ was severe during the haze period. The relative humidity and pH were the key factors influencing SO₄²⁻ formation. We found that NO₃⁻ mainly stemmed from homogeneous gas-phase reactions in the daytime and origi-

* Corresponding authors.

E-mails: panxiaole@mail.iap.ac.cn (X. Pan), wangxiyue1970@163.com (X. Wang).

nated from the hydrolysis of N_2O_5 in the nighttime, which was inconsistent with previous studies. The PMF model identified five sources of $\text{PM}_{2.5}$: secondary origin (37.8%), vehicular emissions (34.7%), biomass burning (11.5%), coal combustion (9.4%), and crustal dust (6.6%).

© 2020 The Research Center for Eco-Environmental Sciences, Chinese Academy of Sciences. Published by Elsevier B.V.

Introduction

Over the past years, China has experienced serious $\text{PM}_{2.5}$ pollution with its rapid economic development, urbanization, and industrialization, especially in the winter on the North China Plain (NCP) (Huang et al., 2014; Zhao et al., 2013; Zhang et al., 2017). In winter, due to intense anthropogenic emissions from coal combustion and biomass burning, unfavorable meteorological conditions, and unique topography, the high aerosol loadings in ambient air were caused by the joint influence of primary source emissions and secondary aerosols (Y. Sun et al., 2013; Cai et al., 2017). Serious $\text{PM}_{2.5}$ pollution impacts regional climate changes and human health (Huang et al., 2014; Jiang et al., 2018; Lelieveld et al., 2015). To understand the characteristics and sources of $\text{PM}_{2.5}$, many studies have investigated the chemical components of $\text{PM}_{2.5}$, especially during the haze episodes in the winter on the NCP, including organic carbon, elemental carbon and water-soluble inorganic ions (WSIs) (Yang et al., 2011; Zheng et al., 2015; Xu et al., 2017; Zou et al., 2018). Previous studies have revealed that sulfate, nitrate, and ammonium (SNA) are the major components of $\text{PM}_{2.5}$ (Dong et al., 2020; Zhang et al., 2018), especially in the haze. In the winter on the NCP, the high relative humidity (RH) promotes the secondary chemical transformation of primary gas precursors (Cheng et al., 2016; Wu et al., 2018; Zhang et al., 2018), and the shallow planetary boundary layer height (PBLH) exacerbates the heavy haze pollution (H. Wang et al., 2019). The dominant secondary inorganic aerosol species changed from sulfate to nitrate, and the main source for the primary organic aerosols changed from coal combustion to biomass burning (Y. Wang et al., 2020).

The cities along the southern foot of the Taihang Mountains, e.g., Zhengzhou and Xinxiang, have been assessed in previous studies. SNA accounted for more than 50% of the $\text{PM}_{2.5}$ mass concentration on haze days in Zhengzhou (S. Wang et al., 2019; Dong et al., 2020). The major chemicals of $\text{PM}_{2.5}$, secondary inorganic aerosols (SIAs), and OC (organic carbon) on polluted days were 2.1–2.3 times higher than those on clean days in Xinxiang (Feng et al., 2018). Jiaozuo (35.17–35.35°N, 113.07–113.43°E) (Fig. 1a), an industrial city in Henan Province, is also located along the southern Taihang Mountains. The administrative area of Jiaozuo covers 4071 km², and the annual coal consumption is approximately 15 million tons, approximately 60% of which is used to generate electricity. In 2017, the annual mass concentration of $\text{PM}_{2.5}$ was 75.7 $\mu\text{g}/\text{m}^3$ in Jiaozuo, which is much higher than the standard of 10 $\mu\text{g}/\text{m}^3$ recommended by the World Health Organization (WHO). In recent years, the Chinese government has firmly decided to improve air quality. The Ministry of Environmental Protection of the People's Republic of China has formulated the scheme of air pollution prevention and con-

trol in the Jing-Jin-Ji Region and surrounding areas in 2017 (Feng et al., 2018). In this scheme, 28 cities are involved, including Jiaozuo. Nevertheless, studies related to $\text{PM}_{2.5}$ about Jiaozuo are rare. Thus, it is urgent to perform relevant research on Jiaozuo. Based on hourly continuous observations of $\text{PM}_{2.5}$, gaseous pollutants, chemical components, and carbonaceous components, we investigated the characteristics, formation mechanism, and sources of $\text{PM}_{2.5}$ in the winter of Jiaozuo. Our findings will help to expand the knowledge of haze formation in NCP and provide some useful information for the improvement of air quality in Jiaozuo.

1. Materials and methods

1.1. Sampling site

Hourly online ambient observations were conducted from December 1, 2017, to February 27, 2018, at the urban site of Jiaozuo (35.10°N, 113.42°E). The observation site is located in the southeast of Jiaozuo (Fig. 1d). There is a trunk road in the eastern site. There are no major sources of pollution nearby. The observations were performed on the third floor of a building, approximately 10 m above the ground. The aerosol optical depth (AOD) was high in Henan Province and in Jiaozuo during the study (Fig. 1b), which indicates that the level of atmospheric aerosol pollution was high. Certain cities near Jiaozuo (Fig. 1c), e.g., Zhengzhou, Luoyang, and Xinxiang, were characterized by serious air pollution as well. This indicates that the $\text{PM}_{2.5}$ observed in Jiaozuo was affected by local sources and regional transportation.

1.2. Instruments

The elemental carbon (EC) and organic carbon (OC) concentrations were measured with a field semicontinuous OCEC aerosol analyzer (Model-4, Sunset Laboratory Inc., USA). The analyzer complies with the NIOSH5040 protocol. The hourly mass concentrations of Mg^{2+} , Ca^{2+} , K^+ , NH_4^+ , Na^+ , SO_4^{2-} , NO_3^- , and Cl^- in $\text{PM}_{2.5}$ were measured with a Monitoring for AeRosols and GAses (MARGA) instrument (ADI 2080, Metrohm Applikon, B.V.). The lowest detection limits of Mg^{2+} , Ca^{2+} , K^+ , NH_4^+ , Na^+ , SO_4^{2-} , NO_3^- , and Cl^- were 0.04, 0.04, 0.09, 0.05, 0.04, 0.04, 0.05 and 0.02 $\mu\text{g}/\text{m}^3$, respectively. The gaseous HNO_3 , HCl , and NH_3 were also measured by MARGA. More details on this instrument can be found in previous studies (ten Brink et al., 2007; Roig Rodelas et al., 2019). The hourly mass concentration of $\text{PM}_{2.5}$ was measured based on the β -ray method (5030i, Thermo Scientific). The hourly mass concentration of SO_2 was measured according to the impulse fluorescence method (43i, Thermo Scientific). The hourly mass concentration of NO_2 was measured with the chemiluminescence method (42i, Thermo

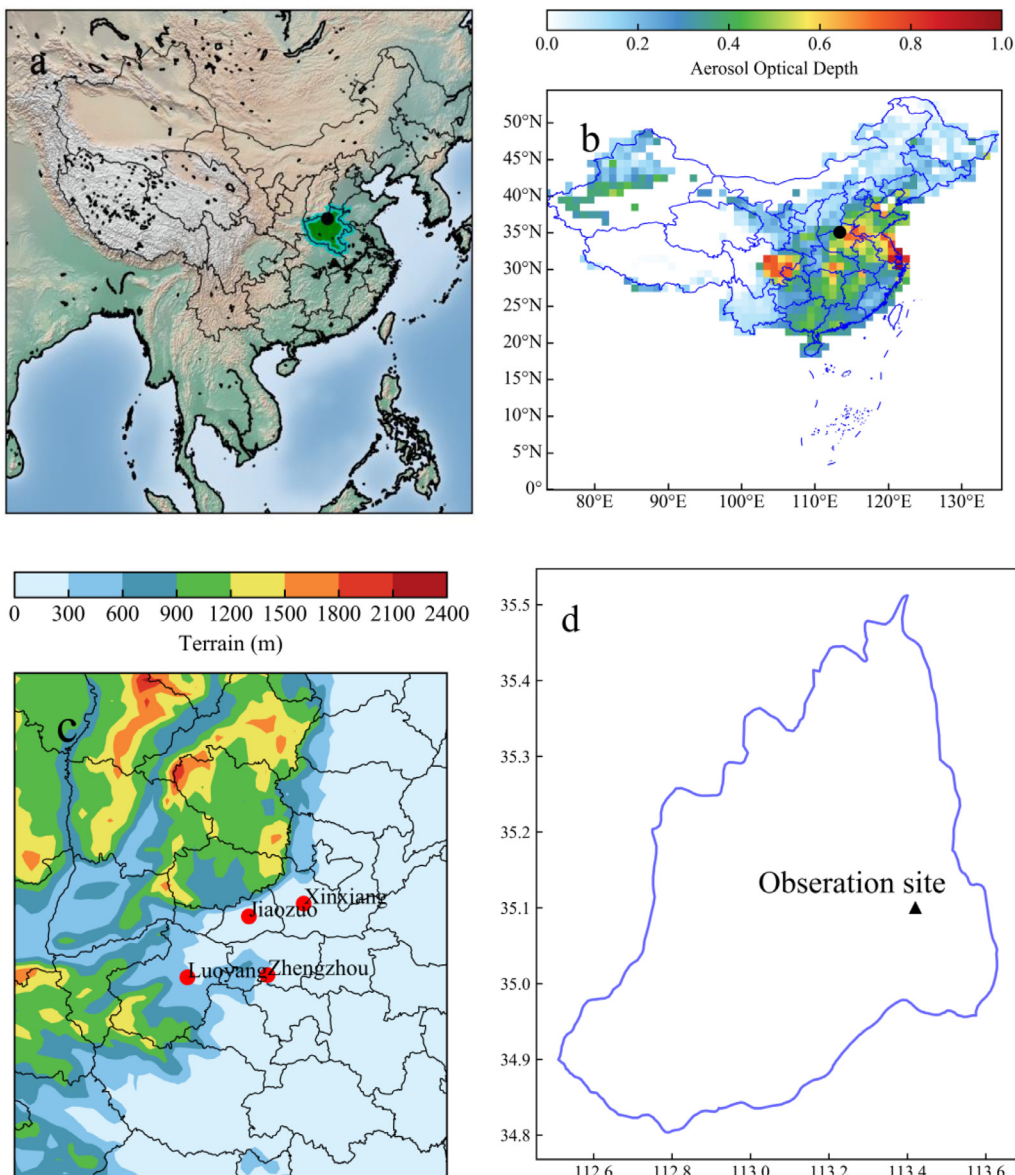


Fig. 1 – (a) Location of Jiaozuo city in China. **(b)** The mean aerosol optical depth (AOD) in China during the whole observation period. **(c)** Location of Jiaozuo and surrounding cities. **(d)** Location of the observation site. The AOD values were retrieved from the MYD04_L2_C6 product of the AOD_550_Dark_Target_Deep_Blue_Combined dataset.

Scientific). The hourly mass concentration of CO was measured following the gas filter correlation (CFC) method (42i, Thermo Scientific). The meteorological parameters, including the wind direction (wd), wind speed (ws), ambient temperature, atmospheric pressure, and relative humidity (RH), were measured at an automatic meteorological station.

1.3. Model calculations

1.3.1. Back trajectory

Backward trajectory analysis is usually employed to identify the potential transport pathways of air masses. With the use of TrajStat software (Wang et al., 2009), 48-hr back trajectories starting at an arrival level of 100 m from the ob-

servation site in Jiaozuo were calculated at a 1-hr resolution during the study period. FNL global analysis data were obtained from the National Center for Environmental Prediction's Global Data Assimilation System (GDAS) wind field reanalysis (<http://www.arl.noaa.gov/>). The backward trajectory model was run every hour of the day. Backward trajectory clustering was then applied to group trajectories with similar geographic origins and histories.

1.3.2. WRF

The Weather Research and Forecasting (WRF) model (version 3.6) was employed to compute the meteorological fields during the observation. The model was configured with two-way nested domains. The grid dimensions were 183×173 and

244×274 , with horizontal resolutions of 45 and 15 km, respectively (Fig. S1). Detailed configurations of the model are provided in Table S1. NCEP FNL reanalysis data, with a $1^\circ \times 1^\circ$ resolution, were adopted to provide the initial and boundary conditions.

1.3.3. Dispersion and trajectory analysis

The air parcel dispersion over Jiaozuo was simulated using the FLEXible PARTicle (FLEXPART) dispersion model. The FLEXPART model (<https://www.flexpart.eu>) developed by the Norwegian Institute for Air Research has been widely used to simulate atmospheric transport processes (Stohl et al., 2005; Tian et al., 2018). This model can perform both forward and backward simulations, which are aimed at tracing particles from source areas and tracking particles from given receptors, respectively (Tian et al., 2018). The WRF outputs of its two simulation domains (described in 1.3.2) were used to drive FLEXPART (Brioude et al., 2013). Thirty-six backward integrations were performed each hour from December 1, 2017, to February 27, 2018. In each integration, 5000 stochastic particles were released at the observation site at a height of 50~100 m. The residence time analysis (RTA) method is applied to determine the relative impacts of the sources in each cell on the receptor (Ashbaugh et al., 1985; Skiles et al., 2018), which is defined as:

$$\text{RTA}(i, j) = \frac{t(i, j)}{T} \times 100\% \quad (1)$$

where, $t(i, j)$ is the residence time in each cell outputted by FLEXPART, and T is the total residence time of all cells.

1.3.4. Positive matrix factorization model

A positive matrix factorization (PMF) model (PMF 5.0) was employed to identify the contribution of sources to samples based on the fingerprints of the sources (Norris and Duvall, 2014). Details on the PMF model can be found in previous studies (Chi et al., 2019; Xie et al., 2020). Ten species were analyzed: eight WSIs, OC, and EC. The concentrations of $\text{PM}_{2.5}$ were also imported into the model to estimate the factor contributing to the total $\text{PM}_{2.5}$. Model parameters were selected according to the user guide and previous studies. Twenty runs were performed for each chemical compound. Between 3 and 6 factors were selected based on the $Q_{\text{robust}}/Q_{\text{true}}$ value.

1.4. pH prediction

The aerosol acidity is the key factor influencing atmospheric chemistry and physics. In this study, we used the ISORROPIA II model to calculate the aerosol pH. ISORROPIA II is a thermodynamic equilibrium model for $\text{Na}^+ \text{-} \text{Cl}^- \text{-} \text{Ca}^{2+} \text{-} \text{K}^+ \text{-} \text{Mg}^{2+} \text{-} \text{SO}_4^{2-} \text{-} \text{NH}_4^+ \text{-} \text{NO}_3^- \text{-} \text{H}_2\text{O}$ aerosol system (Pye et al., 2020). Further descriptions of this model can be found in previous studies (Lin et al., 2020; Shi et al., 2017; Song et al., 2018). In this study, ISORROPIA-II was performed in the forward model for the aerosol system in the metastable condition. The observed hourly concentrations of total ammonium ($\text{NH}_3 + \text{NH}_4^+$), total nitrate ($\text{NO}_3^- + \text{HNO}_3$), total chloride ($\text{Cl}^- + \text{HCl}$), SO_4^{2-} , Na^+ , Ca^{2+} , K^+ , Mg^{2+} , as well as the hourly ambient temperature and RH were served as the input data for ISORROPIA II. The uncertainties of estimated pH by ISORROPIA II under low

RH were high (S. Wang et al., 2020). Thus, the data with $\text{RH} < 30\%$ were excluded in this study.

2. Results and discussion

2.1. General description of the pollutants

2.1.1. Overview of the pollutants and meteorological conditions

As shown in Fig. 2, the mass concentrations of $\text{PM}_{2.5}$ ranged from 5 to $420 \mu\text{g}/\text{m}^3$ with an average of $111 \mu\text{g}/\text{m}^3$, which was much higher than the second grade of the China National Ambient Air Quality Standards (AAQS grade II; $75 \mu\text{g}/\text{m}^3$ on average). In the gaseous pollutants, NO_2 (average: $39 \mu\text{g}/\text{m}^3$), SO_2 (average: $22 \mu\text{g}/\text{m}^3$), and CO (average: $1.3 \text{ mg}/\text{m}^3$) exhibited moderate concentrations. The total mass concentration of the main WSIs in $\text{PM}_{2.5}$, including Mg^{2+} , Ca^{2+} , K^+ , NH_4^+ , Na^+ , SO_4^{2-} , NO_3^- , and Cl^- , during the whole study was $76 \pm 57 \mu\text{g}/\text{m}^3$, accounting for 68% of the $\text{PM}_{2.5}$ mass concentration on average, which was much higher than that observed in the winter in Nanjing (Li et al., 2016; Jiang et al., 2018). The most abundant anions were SO_4^{2-} (13.6%) and NO_3^- (26.9%), and the most abundant cation was NH_4^+ (14.7%). The mass concentrations of OC and EC were 16.8 and $4.2 \mu\text{g}/\text{m}^3$, respectively. In this study, the wind speed ranged from 0~9.5 m/s (average: 3.2 m/s), and the RH ranged from 10% to 90% (average: 42%). The Pearson correlation coefficients between the RH and wind speed and the $\text{PM}_{2.5}$ level were 0.64 and -0.32, respectively. This indicated that a high RH and low wind speed were beneficial to the formation of $\text{PM}_{2.5}$.

2.1.2. Diurnal variation in the pollutants

The diurnal variation in $\text{PM}_{2.5}$ (Fig. 3d) was almost consistent with the diurnal changes in the boundary layer (Fig. S2). There was a $\text{PM}_{2.5}$ peak at 10:00 (LST), which then decreased. At night, the mass concentration of $\text{PM}_{2.5}$ was higher than that during the daytime, which suggested that anthropogenic emissions and aerosol accumulation were relatively high. K^+ , a tracer ion for biomass burning (Andreae et al., 1998), exhibited a peak at approximately 10:00 and 21:00 (LST) (Fig. 3a), corresponding to the rush hours of resident activities, e.g., cooking. A similar phenomenon was reported in Nanjing (Wang et al., 2016). From 00:00 to 3:00 (LST), K^+ concentration was on high-value, which could be related to biomass burning for heating. Ca^{2+} and Mg^{2+} (Fig. 3a, c.), usually associated with windblown, resuspended dust from roads and anthropogenic sources (Nicolas et al., 2009), peaked from 10:00 to 11:00 (LST), which can be the joint effect of road dust during the rush hours and the diurnal variations in the boundary layer (Wang et al., 2016). SO_4^{2-} , NO_3^- and NH_4^+ attained very similar diurnal variations (Fig. 3b, d), indicating that their chemical forms were related (detailed discussion in 2.2.1). Moreover, the fluctuation of the diurnal variations suggested that the associated chemical mechanisms were complex. Most of the WSIs and gaseous pollutants reached low values at approximately 15:00, which could be related to the highest PBLH occurring at this time (Fig. S2).

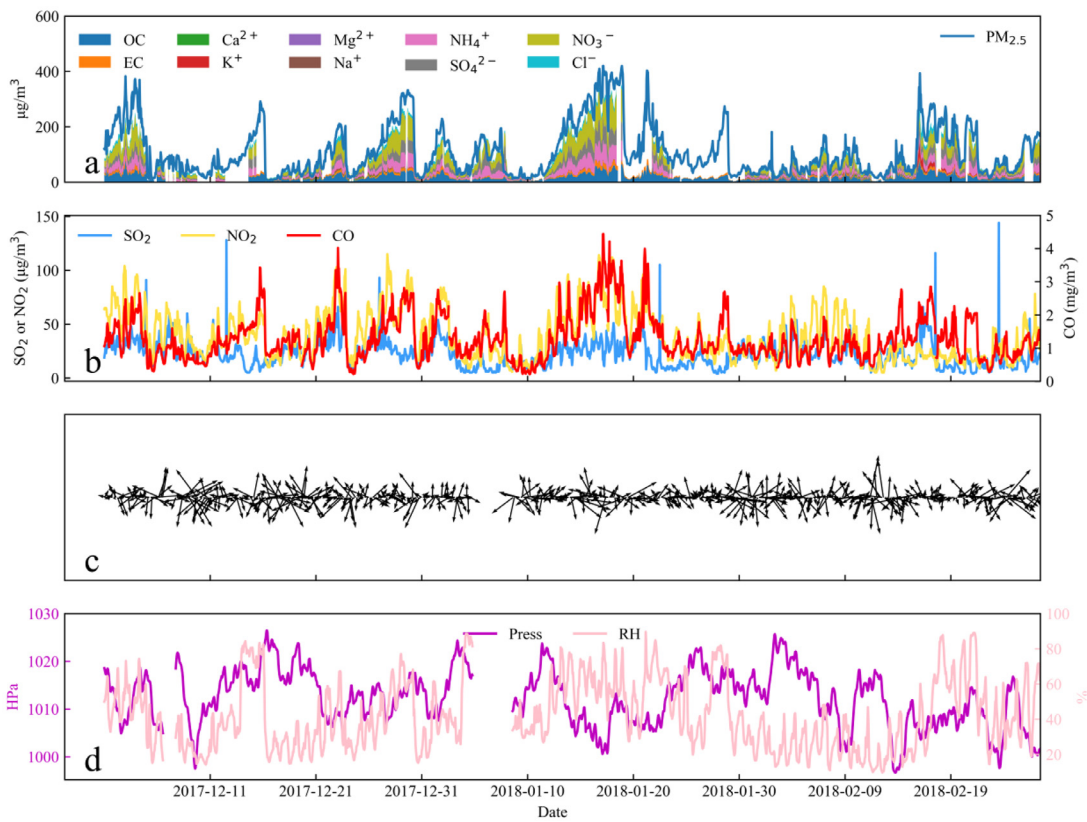


Fig. 2 – Time series of (a) PM_{2.5} and its chemical components, (b) gaseous pollutants, (c) wind speed and wind direction, (d) pressure and RH in Jiaozuo in the winter of 2017.

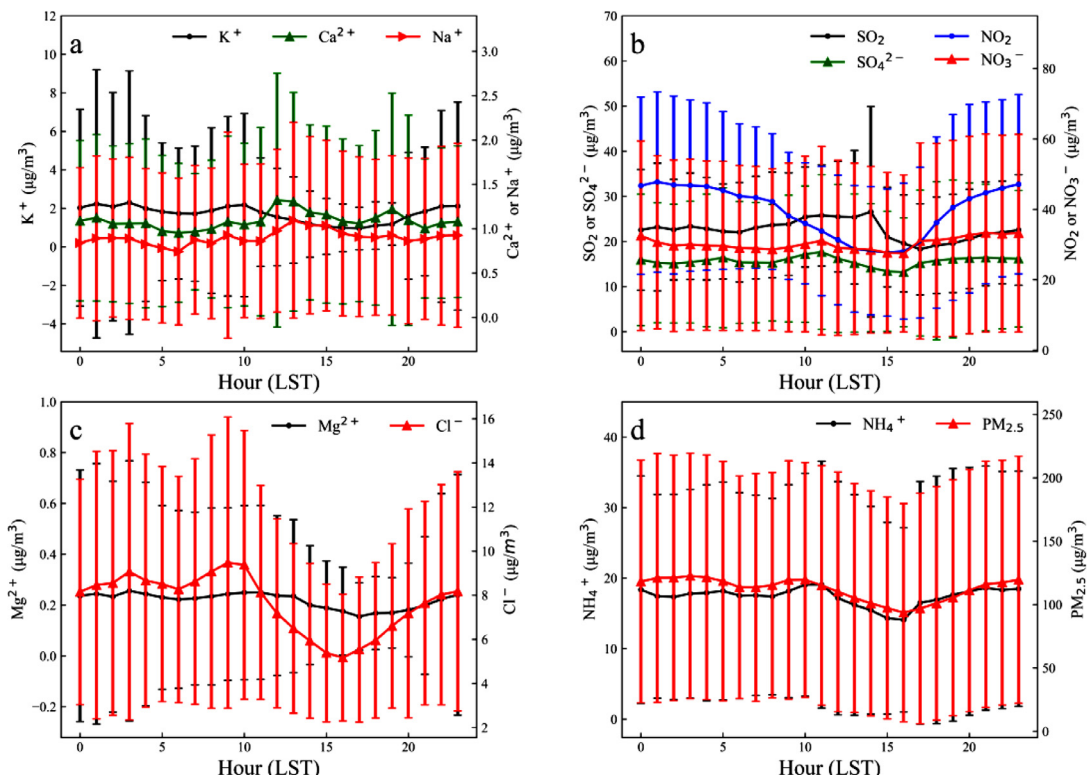


Fig. 3 – Average diurnal variations in the major WSIs, PM_{2.5}, and gaseous pollutants in Jiaozuo in the winter of 2017.

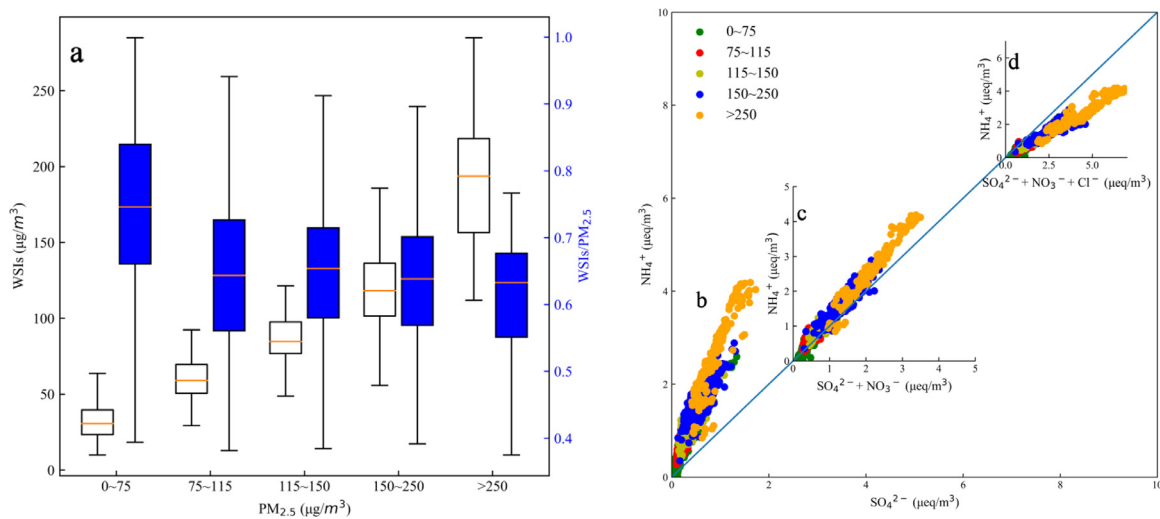


Fig. 4 – (a) Total mass concentration and proportion occupied in $\text{PM}_{2.5}$ of the major water-soluble ions (WSIs) at the different $\text{PM}_{2.5}$ levels; **(b–d)** scatter plot of ammonium vs. the major acidic ions in $\text{PM}_{2.5}$ (electron equivalent concentrations are used).

2.2. Composition, sources and formation mechanism of $\text{PM}_{2.5}$

2.2.1. Composition of $\text{PM}_{2.5}$

As shown in Fig. 4a, the total mass concentration of the major WSIs increased with increasing $\text{PM}_{2.5}$ concentration. The proportion of the major WSIs contained in $\text{PM}_{2.5}$ on clean days ($\text{PM}_{2.5} \leq 75 \mu\text{g}/\text{m}^3$) was higher than that on haze days (Fig. 4a), which indicated that the contribution of the other chemical components increased on haze days. NO_3^- , NH_4^+ , and SO_4^{2-} were the major components of WSIs in descending order, which accounted for 39.7%, 21.7%, and 19.9%, respectively, of the WSIs on average. In previous studies (Ming et al., 2017; Wang et al., 2018), the mass concentration of NH_4^+ was lower than that of SO_4^{2-} , which differed from this study. A higher mass concentration of NO_3^- than that of SO_4^{2-} was found in this study. Over the past decade, owing to the strict control of SO_2 emissions and the sharp increase in motor vehicles (Yang et al., 2015; Fu et al., 2017), the dominant secondary inorganic aerosol species have changed from sulfate to nitrate (Y. Wang et al., 2020).

The homology of the WSIs was analyzed based on hierarchical clustering analysis in this study (Fig. S3). NH_4^+ , SO_4^{2-} , and NO_3^- were clustered into one group. The distance between NH_4^+ and SO_4^{2-} was smaller than that between NH_4^+ and NO_3^- . Generally, SO_4^{2-} is preferentially combined with NH_4^+ over NO_3^- in all chemical models. NH_3 prefers to react with H_2SO_4 to form NH_4HSO_4 or $(\text{NH}_4)_2\text{SO}_4$, and if NH_3 occurs in a sufficient amount for H_2SO_4 , the excess NH_3 could react with HNO_3 to form NH_4NO_3 (Pathak et al., 2009). Fig. 4b–d show scatter plots of NH_4^+ vs. SO_4^{2-} , $\text{SO}_4^{2-} + \text{NO}_3^-$, and $\text{SO}_4^{2-} + \text{NO}_3^- + \text{Cl}^-$ at different $\text{PM}_{2.5}$ levels. Fig. 4b reveals that NH_4^+ is abundant and neutralizes SO_4^{2-} at all $\text{PM}_{2.5}$ levels, which indicates that all SO_4^{2-} exists in the form of $(\text{NH}_4)_2\text{SO}_4$ (Meng et al., 2016). The higher the $\text{PM}_{2.5}$ pollution level is, the more abundant the excess NH_4^+ is. Furthermore, NO_3^- was considered in the charge balance (Fig. 4c). The ratio of NH_4^+ to $\text{SO}_4^{2-} + \text{NO}_3^-$ was above the 1:1 line in most cases, suggest-

ing the presence of NH_4NO_3 and excess NH_4^+ after neutralization by SO_4^{2-} and NO_3^- . The presence of Cl^- fully neutralizes NH_4^+ (Fig. 4d). The remaining Cl^- occurred in the form of KCl (the Pearson coefficient between K^+ and Cl^- was 0.7). In conclusion, SO_4^{2-} , NO_3^- , and Cl^- occurred as $(\text{NH}_4)_2\text{SO}_4$, NH_4NO_3 , NH_4Cl , and KCl.

2.2.2. Source of the WSIs

NO_3^- and SO_4^{2-} are formed via the oxidation of their gaseous precursors (NO_x and SO_2 , respectively). Generally, SO_2 mainly comes from coal combustion, and NO_x primarily stems from vehicle exhaust and fuel combustion (Deng et al., 2016). In this study, $\text{NO}_3^-/\text{SO}_4^{2-}$ (2.1 ± 0.7) was much higher than that in Beijing and Xi'an (Wang et al., 2015; Zhang et al., 2018). During the haze period ($\text{PM}_{2.5} \geq 75 \mu\text{g}/\text{m}^3$), NO_3^- and SO_4^{2-} were higher than those on clean days (Fig. 4b). The sulfur oxidation ratio (SOR) and nitrate oxidation ratio (NOR) can be employed to reflect the degree of atmospheric conversion of SO_2 and NO_2 , respectively, into SO_4^{2-} and NO_3^- , respectively (Fu et al., 2008). SOR and NOR are defined as:

$$\text{SOR} = n\text{SO}_4^{2-} / (n\text{SO}_4^{2-} + n\text{SO}_2) \quad (2)$$

$$\text{NOR} = n\text{NO}_3^- / (n\text{NO}_3^- + n\text{NO}_2) \quad (3)$$

where, n is the molar concentration. The values of SOR (0.30 ± 0.20) and NOR (0.34 ± 0.14) were all much higher than 0.1 in this study, which indicated that the secondary formation of SO_2 into SO_4^{2-} and NO_2 into NO_3^- was notable (Zhang et al., 2018). Generally, agricultural activities are deemed to be the dominant NH_3 sources, accounting for approximately 80% of the global tropospheric NH_3 load (Paulot et al., 2014). In this study, NH_4^+ increased with increasing $\text{PM}_{2.5}$ (Fig. 4b), which was mainly attributed to the increase of NO_3^- and SO_4^{2-} . Additionally, the enhanced NH_3 emissions from fossil fuel combustion and biomass burning (Wu et al., 2020; Xiao et al., 2020a), was a possible cause.

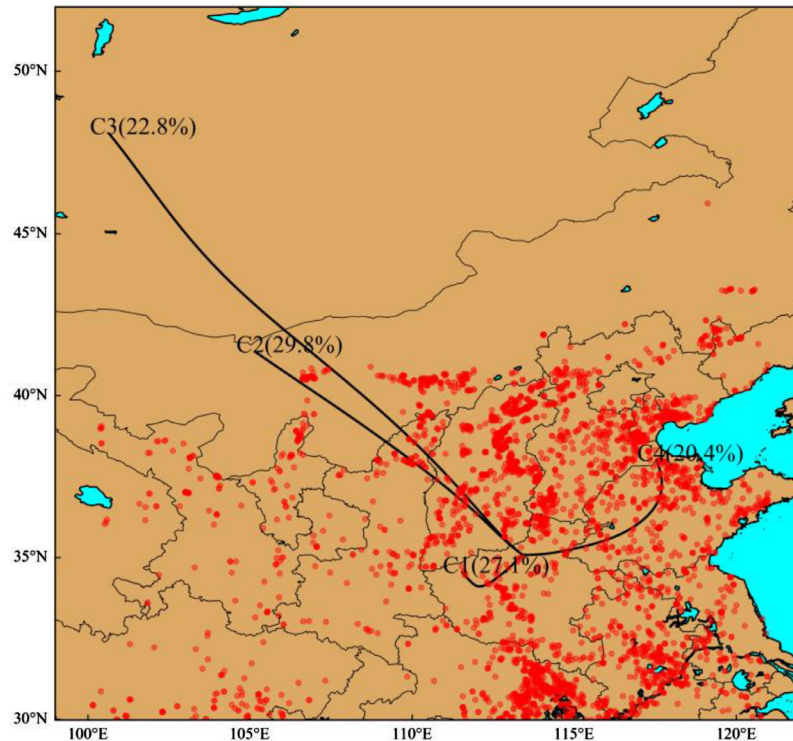


Fig. 5 – Fire map of the areas around Jiaozuo and the trajectory clustering results during the observation period. The fire data were acquired from the Fire Information for Resource Management System (FIRMS) developed by the National Aeronautics and Space Administration (NASA). Moderate Resolution Imaging Spectroradiometer (MODIS) data were used (https://firms.modaps.eosdis.nasa.gov/active_fire/).

The mass concentrations of Mg^{2+} and Ca^{2+} accounted for 0.32% and 2.1%, respectively, of the WSIs in this study. The increasing ratio of Mg^{2+}/Ca^{2+} suggested that Ca^{2+} and Mg^{2+} are affected by anthropogenic sources (Guo et al., 2020). The Mg^{2+}/Ca^{2+} ratio was 0.18 in Jiaozuo, which was much higher than that observed in Kunming (0.02 to 1.91) (Guo et al., 2020). The Mg^{2+}/Ca^{2+} ratio on haze days was approximately four times as high as that on clean days in Jiaozuo, which indicated that anthropogenic emissions contributed to the observed haze.

The proportions of Cl^- and K^+ were much lower than those of SO_4^{2-} and NO_3^- . Sea salt, coal combustion, and biomass burning are sources of Cl^- (Z. Sun et al., 2013). Jiaozuo is an inland city, and the nearest sea is more than 500 km away. We deduced that sea salt contributed little to Cl^- , and Cl^- originated from coal combustion or/and biomass burning. K^+ , as a tracer of biomass burning (Andreae et al., 1998; Gao et al., 2011), has been widely found to be the result of biomass burning. In our results, a strong correlation between K^+ and Cl^- ($r = 0.70$, $p < 0.01$) and a moderate correlation between Cl^- and SO_2 ($r = 0.5$, $p < 0.01$) were found. This indicated that biomass burning and coal combustion were the main sources of Cl^- and K^+ , respectively, in Jiaozuo. As shown in Fig. 5, the wildfires around Jiaozuo, especially in areas above which air masses passed, were intensive, thus confirming our results. The mean ratio of OC to EC was 4.84 in this study, which approached the threshold value between biomass burning and vehicle emissions (Ji et al., 2019).

2.2.3. Formation path of SO_4^{2-} and NO_3^-

As described above, serious oxidation of SO_2 and NO_2 occurred during the haze period. Furthermore, we investigated the formation path of SO_4^{2-} and NO_3^- . The average SOR (0.30) in Jiaozuo was much higher than that in Handan (0.1) and Zhengzhou (0.23) (Table 1). The SOR on haze days ($PM_{2.5} \geq 75 \mu g/m^3$) was approximately twice as high as that on clean days ($PM_{2.5} \leq 75 \mu g/m^3$), which indicated more intensive secondary transformation on the haze days. Atmospheric sulfate mainly originates from the SO_2 oxidation pathway, including gas-phase reactions with OH radicals or stabilized Criegee intermediates, heterogeneous-phase reactions on the surface of particles, and aqueous-phase reactions with dissolved O_3 , NO_2 , H_2O_2 , and organic peroxides (Liu et al., 2020). In previous studies, a high RH promotes SO_2 oxidation. The mean values of the SOR increased remarkably when the RH was above 40% in this study (Fig. 6b), which was similar to previous findings (Liu et al., 2019, 2020). At a low RH, the SO_2 oxidation pathway could include gas-phase reactions and heterogeneous reactions. When the RH was high (> 60%), SO_4^{2-} primarily stemmed from the aqueous oxidation of SO_2 due to aerosol water content and surface area increase (Zhang et al., 2015). The aerosol acidity is a key factor influencing the aqueous oxidation pathways (Zhang et al., 2018; Liu et al., 2020). The mean evaluated pH was 5.46 ± 0.69 in this study, which was higher than that in Zhengzhou (4.5) (S. Wang et al., 2020). This indicated that the acids in the aerosols in Jiaozuo city were more neutralized. As shown in Fig. 6a, the aerosols pH

Table 1 – Sulfur oxidation ratio (SOR) and nitrate oxidation ratio (NOR) in different studies.

Date	Site	SOR	NOR	References
2015.02.10~2015.03.19	Urban site in Beijing, China	0.27	0.17	Zhang et al., 2018
The winter of 2013 and 2014	Handan, China	0.1	0.2	Meng et al., 2016
2017.12.01~2018.02.28	Zhengzhou, China	0.23	0.24	Yang et al., 2020
The winter of 2017	Taiwan, China	0.31	0.11	Shen et al., 2020
2017.12.01~2018.02.28	Jiaozuo, China	0.30	0.34	This study

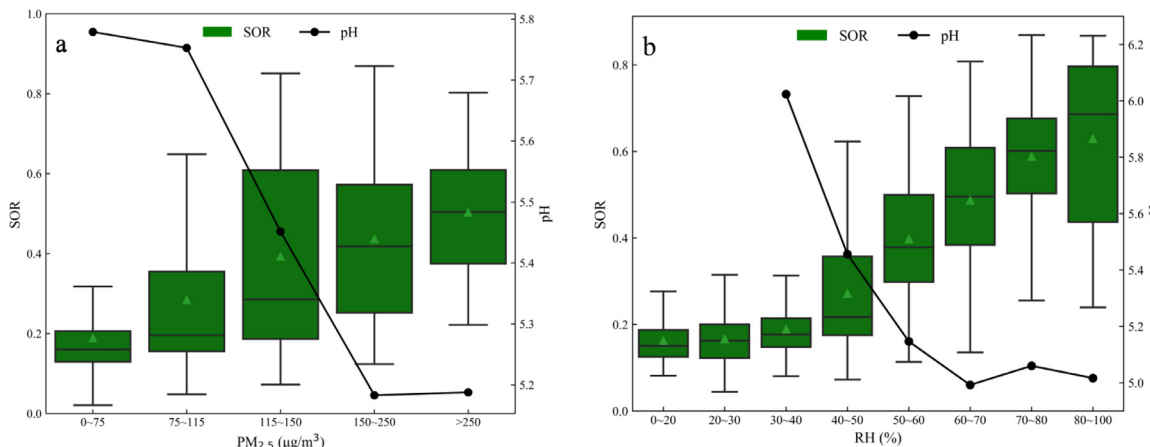


Fig. 6 – (a) Sulfur oxidation ratio (SOR) and pH at the different levels of PM_{2.5}; (b) SOR and pH at the different RH levels. The mean (triangles within the boxes), median (central horizontal bars within the boxes), 25th and 75th percentiles (lower and upper bars, respectively, of the boxes), and minimum and maximum values (lower and upper whiskers, respectively) are indicated.

decreased as the increase of PM_{2.5} mass concentration. It is believed that a relatively high RH and low pH are beneficial to the aqueous phase chemistry of sulfate formation (Liu et al., 2017, 2020). RH was negatively correlated with pH aerosol in this study ($r = -0.56$) (Fig. 6b), which suggested high aerosol water content was responsible for the relatively lower aerosol pH (Liu et al., 2017).

The average NOR (0.34) in this study was much higher than that in Zhengzhou and Handan (Table 1), which indicated a more intensive secondary formation of nitrate in Jiaozuo. The NOR value increased with increasing PM_{2.5} concentration, and the NOR was not related to the NO₂ concentration (Fig. 7a). NO_x transformation was more pronounced during the haze episodes than during the clean periods in Jiaozuo. The correlation between the NOR and RH ($r = 0.46$, $p < 0.01$) was less notable than that between the SOR and RH ($r = 0.79$, $p < 0.01$), which suggested that NO₃⁻ formation was less sensitive to the RH than to SO₄²⁻. The NO₃⁻ formation pathway mainly includes NO₂ oxidation by OH radicals in the gas phase, heterogeneous reactions on the particle surface, and heterogeneous hydrolysis of N₂O₅ on wet aerosols or chloride-containing aerosols (He et al., 2014; Liu et al., 2020). As shown in Fig. 7b, during the daytime (10:00–15:00), the RH gradually decreased with increasing solar radiation, but the NOR and NO₃⁻/PM_{2.5} sharply increased. RH reduction is unfavorable to heterogeneous reactions. This indicated that during the daytime, NO₃⁻ mainly originated from the homogeneous gas-phase reactions of NO₂ and OH radicals rather than het-

erogeneous reactions (Xiao et al., 2020b; Ye et al., 2019). At night, NO₃⁻ mainly stemmed from the hydrolysis of N₂O₅ on the aerosol surface (Xiao et al., 2020b; Zhang et al., 2018).

2.3. Source identify

2.3.1. Source apportionment of the WSIs

Five sources of the PM_{2.5} concentration were identified based on the PMF model (Fig. 8), including the secondary origin (37.8%), vehicular emissions (34.7%), biomass burning (11.5%), coal combustion (9.4%), and crustal dust (6.6%).

Factor 1 was weighted by K⁺ and was treated as biomass burning. Factor 2 exhibited high loadings for NH₄⁺, SO₄²⁻, and NO₃⁻, which can be identified as a secondary origin. Factor 3 was characterized by high contributions of OC and EC, which mainly originates from gasoline and diesel-burning (Li et al., 2020). Therefore, factor 3 was designated as vehicular emissions. High Ca²⁺ and Mg²⁺ levels occurred in factor 4, which is regarded as crustal dust. The chemical profile of factor 5 was mainly characterized by Na⁺. Jiaozuo is an inland city; thus, sea salt is not the main source of Na⁺. This factor is identified as coal combustion.

2.3.2. Geographical origins of the pollutants

Fig. 9 and S4 show the mean RTA values for the different WSIs. NH₄⁺, SO₄²⁻, and NO₃⁻ have similar distribution characteristics (Fig. 9a, S4a, b), respectively, with high RTA values mainly occurring in the northwest areas of the monitoring site. Henan

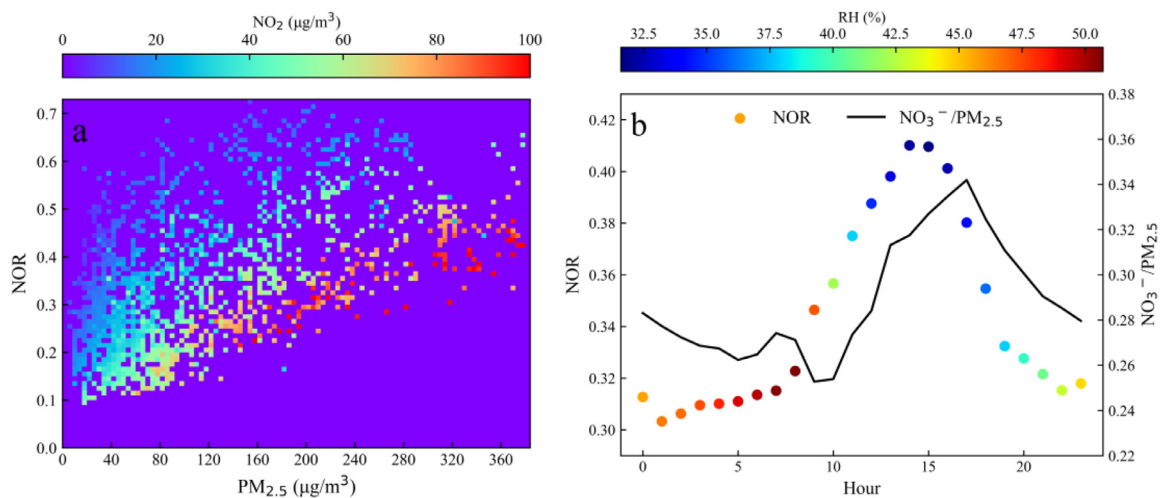


Fig. 7 – (a) Relationship between the $\text{PM}_{2.5}$ concentration and nitrate oxidation ratio (NOR) (the contour color indicates the NO_2 concentration), **(b)** diurnal variation in NOR and $\text{NO}_3^-/\text{PM}_{2.5}$.

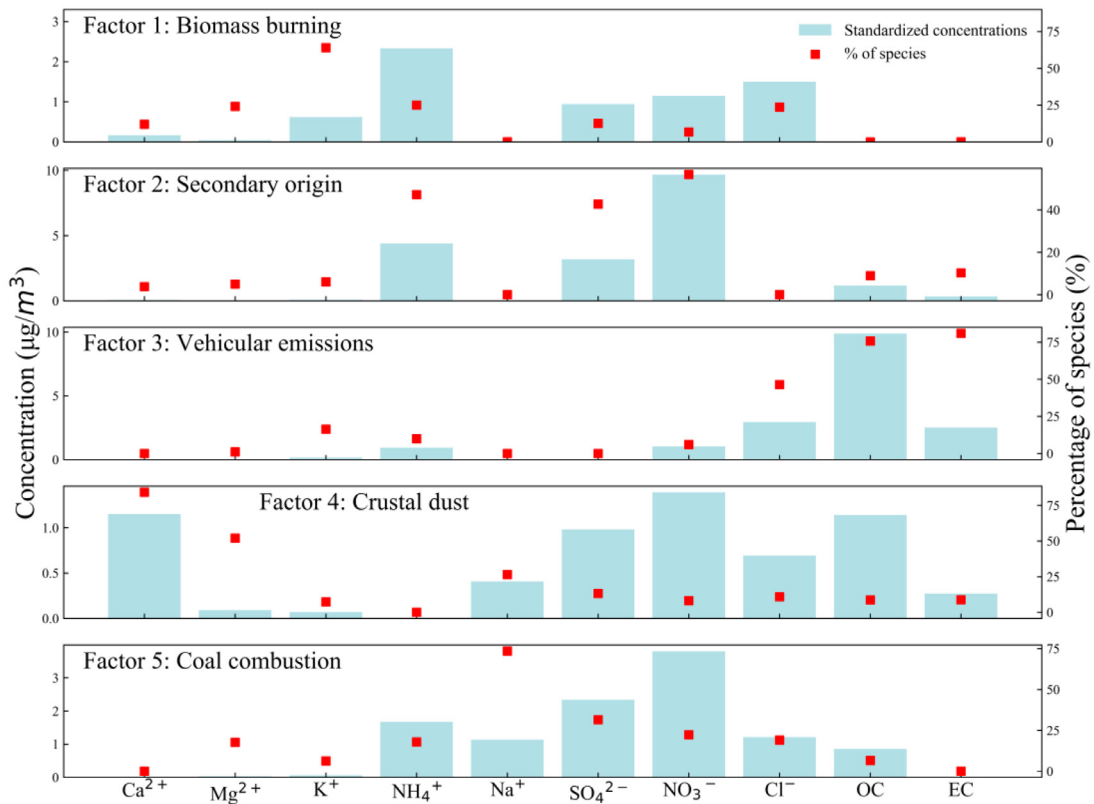


Fig. 8 – Source profiles of $\text{PM}_{2.5}$ during the study period. The red points mark the dominant species characterizing each factor profile.

and Shanxi Provinces also experience high pollutant emissions and air pollution levels (Wei et al., 2018; H. Yang et al., 2020). This indicated that secondary pollutants from Shanxi Province could impact Jiaozuo. As shown in Fig. 9b, K^+ had high RTA values in the northwestern and northeastern areas of the monitoring site, which was consistent with Mg^{2+} (Fig. S4c). During the study, there were intense wildfires in

these areas (Fig. 5). This suggested that the pollutants emitted by biomass burning in Shanxi Province and northeastern Henan Province, e.g., Zhengzhou, Xinxiang, and Anyang, could influence Jiaozuo. Ca^{2+} displayed high RTA values in the northwestern and southwestern parts of Jiaozuo. This indicated that Jiaozuo city could be affected by dust sources from southern Shanxi Province and northwestern Henan Province.

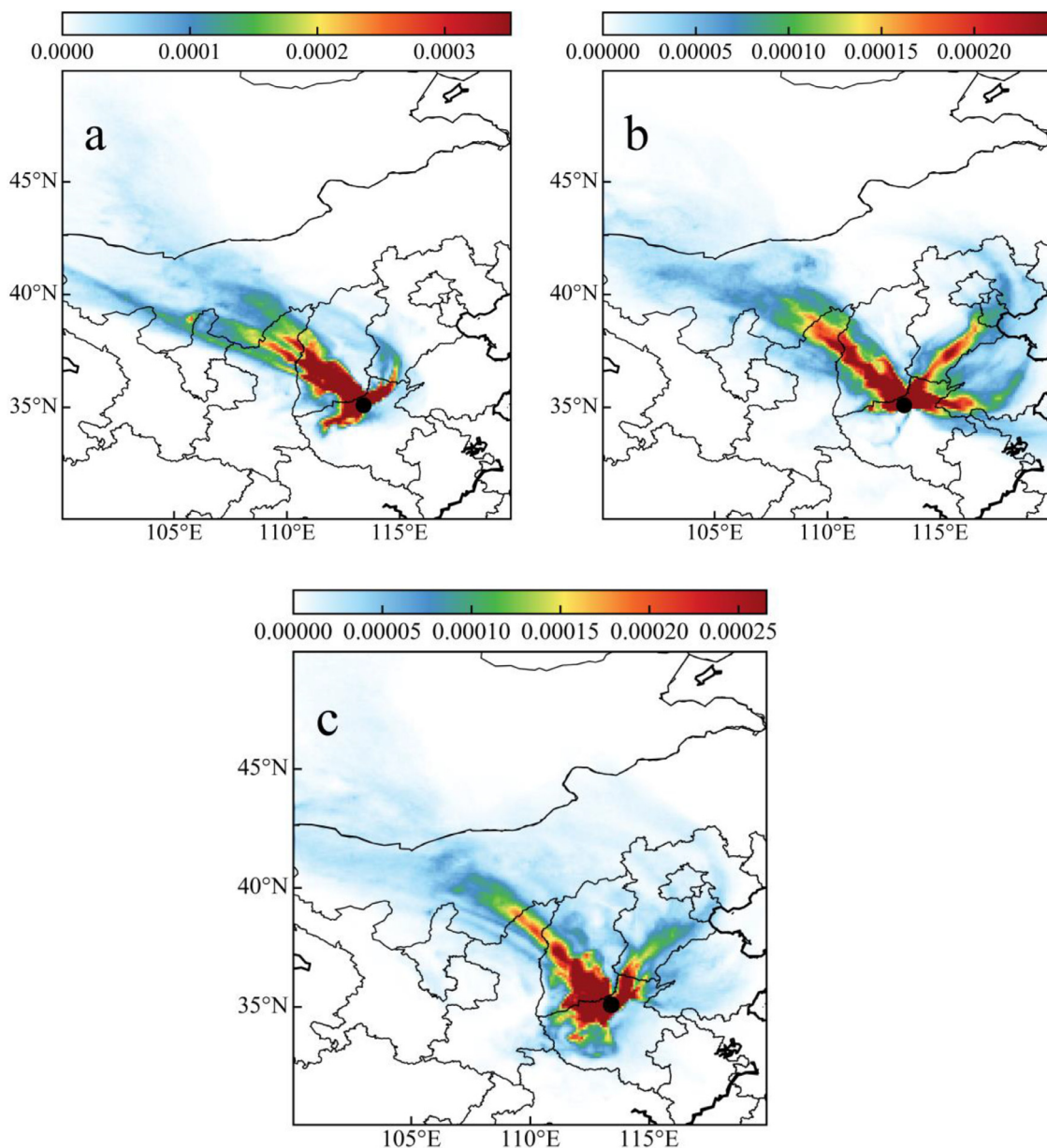


Fig. 9 – Mean residence time analysis (RTA) values for (a) NO_3^- , (b) K^+ , and (c) Ca^{2+} at a mass concentration above the 90th percentile.

In summary, the air pollutants in Jiaozuo mainly originated from local sources and pollutant transport from surrounding cities, which emphasizes that it is very important to implement measures of regional cooperation and joint defense and control strategies.

3. Conclusions

The chemical characteristics, formation mechanism, and sources of the $\text{PM}_{2.5}$ in Jiaozuo were examined in detail in this study based on hourly measurements from December 1, 2017, to February 28, 2018. During the whole observation period, the average mass concentration of $\text{PM}_{2.5}$ was $111 \mu\text{g}/\text{m}^3$, which suggested serious haze pollution in Jiaozuo. The total mass

concentration of the WSIs accounted for 68% of the $\text{PM}_{2.5}$ mass concentration on average. The WSIs and $\text{PM}_{2.5}$ exhibited distinct diurnal variations under the joint effects of the boundary layer and emission sources. NO_3^- , NH_4^+ , and SO_4^{2-} were the major components of the WSIs in descending order, which accounted for 40%, 22%, and 20%, respectively, of the WSIs on average. SO_4^{2-} , NO_3^- , and Cl^- occurred in the form of $(\text{NH}_4)_2\text{SO}_4$, NH_4NO_3 , NH_4Cl , and KCl in Jiaozuo. The SOR (0.30) and NOR (0.34) in Jiaozuo were much higher than those in other cities in China, which indicated notable oxidation of SO_2 and NO_2 . At a low RH, sulfate mainly originated from gas-phase and heterogeneous reactions. When the RH was high ($>60\%$), sulfate mainly came from the aqueous oxidation of SO_2 . The aqueous phase chemistry of sulfate formation was enhanced at low pH and high RH. NO_3^- mainly stemmed from homogeneous gas-

phase reactions during the daytime and originated from the hydrolysis of N_2O_5 during the nighttime. The PMF model identified five sources of $\text{PM}_{2.5}$: secondary origin (37.8%), vehicular emissions (34.7%), biomass burning (11.5%), coal combustion (9.4%), and crustal dust (6.6%). The FLEXPART model results revealed that the air pollutants in Jiaozuo mainly came from local sources and pollutant transport from surrounding cities.

Acknowledgments

This work was sponsored by the Strategic Priority Research Program of the Chinese Academy of Sciences (No. Grant XDA19040201) and the National Natural Science Foundation of China (No. 41877314). The authors acknowledge the Institute of Atmospheric Physics for providing the research platform.

Appendix A Supplementary data

Supplementary material associated with this article can be found, in the online version, at doi:[10.1016/j.jes.2020.10.004](https://doi.org/10.1016/j.jes.2020.10.004).

REFERENCES

- Andreae, M.O., Andreae, T.W., Annegarn, H., Beer, J., Cachier, H., le Canut, P., et al., 1998. Airborne studies of aerosol emissions from savanna fires in Southern Africa: 2. aerosol chemical composition. *J. Geophys. Res.-Atmos.* 103, 32119–32128.
- Ashbaugh, L.L., Malm, W.C., Sadeh, W.Z., 1985. A residence time probability analysis of sulfur concentrations at Grand-Canyon-National-Park. *Atmos. Environ.* 19, 1263–1270.
- Brioude, J., Arnold, D., Stohl, A., Cassiani, M., Morton, D., Seibert, P., et al., 2013. The lagrangian particle dispersion model Flexpart-WRF version 3.1. *Geosci. Model Dev.* 6, 1889–1904.
- Cai, W.J., Li, K., Liao, H., Wang, H.J., Wu, L.X., 2017. Weather conditions conducive to Beijing severe haze more frequent under climate change. *Nat. Clim. Chang.* 7, 257–262.
- Cheng, Y., Zheng, G., Wei, C., Mu, Q., Zheng, B., Wang, Z., et al., 2016. Reactive nitrogen chemistry in aerosol water as a source of sulfate during haze events in China. *Sci. Adv.* 2, e1601530.
- Chi, R., Li, H.Y., Wang, Q., Zhai, Q.R., Wang, D.D., Wu, M., et al., 2019. Association of emergency room visits for respiratory diseases with sources of ambient $\text{PM}_{2.5}$. *J. Environ. Sci.* 86, 154–163.
- Deng, X.L., Shi, C.E., Wu, B.W., Yang, Y.J., Jin, Q., Wang, H.L., et al., 2016. Characteristics of the water-soluble components of aerosol particles in Hefei, China. *J. Environ. Sci.* 42, 32–40.
- Dong, Z.S., Su, F.C., Zhang, Z.Y., Wang, S.B., 2020. Observation of chemical components of $\text{PM}_{2.5}$ and secondary inorganic aerosol formation during haze and sandy haze days in Zhengzhou, China. *J. Environ. Sci.* 88, 316–325.
- Feng, J.L., Yu, H., Mi, K., Su, X.F., Li, Y., Li, Q.L., et al., 2018. One year study of $\text{PM}_{2.5}$ in Xinxiang City, North China: seasonal characteristics, climate impact and source. *Ecotox. Environ. Safe.* 154, 75–83.
- Fu, Q.Y., Zhuang, G.S., Wang, J., Xu, C., Huang, K., Li, J., et al., 2008. Mechanism of formation of the heaviest pollution episode ever recorded in the Yangtze River Delta, China. *Atmos. Environ.* 42, 2023–2036.
- Fu, X., Wang, S.X., Xing, J., Zhang, X.Y., Wang, T., Hao, J.M., 2017. Increasing ammonia concentrations reduce the effectiveness of particle pollution control achieved via SO_2 and NO_x emissions reduction in east China. *Environ. Sci. Technol. Lett.* 4, 221–227.
- Gao, X.M., Yang, L.X., Cheng, S.H., Gao, R., Zhou, Y., Xue, L.K., et al., 2011. Semi-continuous measurement of water-soluble ions in $\text{PM}_{2.5}$ in Jinan, China: temporal variations and source apportionments. *Atmos. Environ.* 45, 6048–6056.
- Guo, W., Zhang, Z.Y., Zheng, N.J., Luo, L., Xiao, H.Y., Xiao, H.W., 2020. Chemical characterization and source analysis of water-soluble inorganic ions in $\text{PM}_{2.5}$ from a plateau city of Kunming at different seasons. *Atmos. Res.* 234, 104687.
- He, H., Wang, Y.S., Ma, Q.X., Ma, J.Z., Chu, B.W., Ji, D.S., et al., 2014. Mineral dust and NO_x promote the conversion of SO_2 to sulfate in heavy pollution days. *Sci. Rep.* 4, 5.
- Huang, R.J., Zhang, Y.L., Bozzetti, C., Ho, K.F., Cao, J.J., Han, Y.M., et al., 2014. High secondary aerosol contribution to particulate pollution during haze events in China. *Nature* 514 (7521), 218–222.
- Ji, D.S., Gao, M., Maenhaut, W., He, J., Wu, C., Cheng, L.J., et al., 2019. The carbonaceous aerosol levels still remain a challenge in the Beijing-Tianjin-Hebei region of China: insights from continuous high temporal resolution measurements in multiple cities. *Environ. Int.* 126, 171–183.
- Jiang, N., Yin, S.S., Guo, Y., Li, J.Y., Kang, P.R., Zhang, R.Q., et al., 2018. Characteristics of mass concentration, chemical composition, source apportionment of $\text{PM}_{2.5}$ and PM_{10} and health risk assessment in the emerging megacity in China. *Atmos. Pollut. Res.* 9, 309–321.
- Lelieveld, J., Evans, J.S., Fnais, M., Giannadaki, D., Pozzer, A., 2015. The contribution of outdoor air pollution sources to premature mortality on a global scale. *Nature* 525 (7569), 367–371.
- Li, H.M., Wang, Q.G., Yang, M., Li, F.Y., Wang, J.H., Sun, Y.X., et al., 2016. Chemical characterization and source apportionment of $\text{PM}_{2.5}$ aerosols in a megacity of Southeast China. *Atmos. Res.* 181, 288–299.
- Li, Y., Liu, B., Xue, Z., Zhang, Y., Sun, X., Song, C., et al., 2020. Chemical characteristics and source apportionment of $\text{PM}_{2.5}$ using PMF modelling coupled with 1-hr resolution online air pollutant dataset for Linfen, China. *Environ. Pollut.* 263, 114532.
- Lin, Y.C., Zhang, Y.L., Fan, M.Y., Bao, M.Y., 2020. Heterogeneous formation of particulate nitrate under ammonium-rich regimes during the high- $\text{PM}_{2.5}$ events in Nanjing, China. *Atmos. Chem. Phys.* 20, 3999–4011.
- Liu, M.X., Song, Y., Zhou, T., Xu, Z.Y., Yan, C.Q., Zheng, M., et al., 2017. Fine particle pH during severe haze episodes in Northern China. *Geophys. Res. Lett.* 44, 5213–5221.
- Liu, P.F., Ye, C., Xue, C.Y., Zhang, C.L., Mu, Y.J., Sun, X., 2020. Formation mechanisms of atmospheric nitrate and sulfate during the winter haze pollution periods in Beijing: gas-phase, heterogeneous and aqueous-phase chemistry. *Atmos. Chem. Phys.* 20, 4153–4165.
- Liu, Z.R., Hu, B., Ji, D.S., Cheng, M.T., Gao, W.K., Shi, S.Z., et al., 2019. Characteristics of fine particle explosive growth events in Beijing, China: seasonal variation, chemical evolution pattern and formation mechanism. *Sci. Total Environ.* 687, 1073–1086.
- Meng, C.C., Wang, L.T., Zhang, F.F., Wei, Z., Ma, S.M., Ma, X., et al., 2016. Characteristics of concentrations and water-soluble inorganic ions in $\text{PM}_{2.5}$ in Handan City, Hebei Province, China. *Atmos. Res.* 171, 133–146.
- Ming, L.L., Jin, L., Li, J., Fu, P.Q., Yang, W.Y., Liu, D., et al., 2017. $\text{PM}_{2.5}$ in the Yangtze river Delta, China: chemical compositions, seasonal variations, and regional pollution events. *Environ. Pollut.* 223, 200–212.
- Nicolas, J.F., Galindo, N., Yubero, E., Pastor, C., Esclapez, R., Crespo, J., 2009. Aerosol inorganic ions in a semiarid region on the Southeastern Spanish Mediterranean coast. *Water Air Soil Pollut.* 201, 149–159.
- Norris, G., Duvall, R., 2014. Positive Matrix Factorization (PMF) 5.0 Fundamentals & User guide, U.S. Environmental Protection Agency, Washington, DC, USA.

- Pathak, R.K., Wu, W.S., Wang, T., 2009. Summertime PM_{2.5} ionic species in four major cities of China: nitrate formation in an ammonia-deficient atmosphere. *Atmos. Chem. Phys.* 9, 1711–1722.
- Paulot, F., Jacob, D.J., Pinder, R.W., Bash, J.O., Travis, K., Henze, D.K., 2014. Ammonia emissions in the United States, European Union, and China derived by high-resolution inversion of ammonium wet deposition data: interpretation with a new agricultural emissions inventory (MASAGE_NH₃). *J. Geophys. Res.-Atmos.* 119, 4343–4364.
- Pye, H.O.T., Nenes, A., Alexander, B., Ault, A.P., Barth, M.C., Clegg, S.L., et al., 2020. The acidity of atmospheric particles and clouds. *Atmos. Chem. Phys.* 20, 4809–4888.
- Rodelas, Roig, R., Perdrix, E., Herbin, B., Riffault, 2019. Characterization and variability of inorganic aerosols and their gaseous precursors at a suburban site in Northern France over one year (2015–2016). *Atmos. Environ.* 200, 142–157.
- Shen, H.Z., Cheng, P.H., Yuan, C.S., Yang, Z.M., Hung, C.M., Yen, P.H., et al., 2020. Chemical characteristics, spatiotemporal distribution, and source apportionment of PM_{2.5} surrounding industrial complexes in Southern Kaohsiung. *Aerosol Air Qual. Res.* 20, 557–575.
- Shi, G.L., Xu, J., Peng, X., Xiao, Z.M., Chen, K., Tian, Y.Z., et al., 2017. pH of aerosols in a polluted atmosphere: source contributions to highly acidic aerosol. *Environ. Sci. Technol.* 51, 4289–4296.
- Skiles, M.J., Lai, A.M., Olson, M.R., Schauer, J.J., de Foy, B., 2018. Source apportionment of PM_{2.5} organic carbon in the San Joaquin Valley using monthly and daily observations and meteorological clustering. *Environ. Pollut.* 237, 366–376.
- Song, S.J., Gao, M., Xu, W.Q., Shao, J.Y., Shi, G.L., Wang, S.X., et al., 2018. Fine-particle pH for Beijing winter haze as inferred from different thermodynamic equilibrium models. *Atmos. Chem. Phys.* 18, 7423–7438.
- Stohl, A., Forster, C., Frank, A., Seibert, P., Wotawa, G., 2005. Technical note: the lagrangian particle dispersion model flexpart version 6.2. *Atmos. Chem. Phys.* 5, 2461–2474.
- Sun, Y.L., Wang, Z.F., Fu, P.Q., Yang, T., Jiang, Q., Dong, H.B., et al., 2013a. Aerosol composition, sources and processes during wintertime in Beijing, China. *Atmos. Chem. Phys.* 13, 4577–4592.
- Sun, Z.Q., Mu, Y.J., Liu, Y.J., Shao, L.Y., 2013b. A comparison study on airborne particles during haze days and non-haze days in Beijing. *Sci. Total Environ.* 456, 1–8.
- ten Brink, H., Otjes, R., Jongejan, P., Slanina, S., 2007. An instrument for semi-continuous monitoring of the size-distribution of nitrate, ammonium, sulphate and chloride in aerosol. *Atmos. Environ.* 41, 2768–2779.
- Tian, Y., Pan, X., Nishizawa, T., Kobayashi, H., Uno, I., Wang, X., et al., 2018. Variability of depolarization of aerosol particles in the megacity of Beijing: implications for the interaction between anthropogenic pollutants and mineral dust particles. *Atmos. Chem. Phys.* 18, 18203–18217.
- Wang, H., Li, Z., Lv, Y., Xu, H., Li, K., Li, D., et al., 2019a. Observational study of aerosol-induced impact on planetary boundary layer based on lidar and sunphotometer in Beijing. *Environ. Pollut.* 252, 897–906.
- Wang, H.L., An, J.L., Cheng, M.T., Shen, L.J., Zhu, B., Li, Y., et al., 2016. One year online measurements of water-soluble ions at the industrially polluted town of Nanjing, China: sources, seasonal and diurnal variations. *Chemosphere* 148, 526–536.
- Wang, P., Cao, J.J., Shen, Z.X., Han, Y.M., Lee, S.C., Huang, Y., et al., 2015. Spatial and seasonal variations of PM_{2.5} mass and species during 2010 in Xi'an, China. *Sci. Total Environ.* 508, 477–487.
- Wang, S.B., Wang, L.L., Li, Y.Q., Wang, C., Wang, W.S., Yin, S.S., et al., 2020a. Effect of ammonia on fine-particle pH in agricultural regions of China: comparison between urban and rural sites. *Atmos. Chem. Phys.* 20, 2719–2734.
- Wang, S.B., Yin, S.S., Zhang, R.Q., Yang, L.M., Zhao, Q.Y., Zhang, L.S., et al., 2019b. Insight into the formation of secondary inorganic aerosol based on high-time-resolution data during haze episodes and snowfall periods in Zhengzhou, China. *Sci. Total Environ.* 660, 47–56.
- Wang, W., Yua, J., Cui, Y., He, J., Xue, P., Cao, W., et al., 2018. Characteristics of fine particulate matter and its sources in an industrialized coastal city, Ningbo, Yangtze River Delta, China. *Atmos. Res.* 203, 105–117.
- Wang, Y.C., Wang, Q.Y., Ye, J.H., Li, L., Zhou, J., Ran, W.K., et al., 2020b. Chemical composition and sources of submicron aerosols in winter at a regional site in Beijing-Tianjin-Hebei region: implications for the joint action plan. *Sci. Total Environ.* 719, 137547.
- Wang, Y.Q., Zhang, X.Y., Draxler, R.R., 2009. Trajstat: gis-based software that uses various trajectory statistical analysis methods to identify potential sources from long-term air pollution measurement data. *Environ. Model. Softw.* 24, 938–939.
- Wei, W.X., Li, P., Wang, H.Q., Song, M.L., 2018. Quantifying the effects of air pollution control policies: a case of Shanxi Province in China. *Atmos. Pollut. Res.* 9, 429–438.
- Wu, C., Wang, G., Li, J., Li, J., Cao, C., Ge, S., et al., 2020. Non-agricultural sources dominate the atmospheric NH₃ in Xi'an, a megacity in the semi-arid region of China. *Sci. Total Environ.* 722, 137756.
- Wu, Z.J., Wang, Y., Tan, T.Y., Zhu, Y.S., Li, M.R., Shang, D.J., et al., 2018. Aerosol liquid water driven by anthropogenic inorganic salts: implying its key role in haze formation over the North China Plain. *Environ. Sci. Technol. Lett.* 5, 160–166.
- Xiao, H.W., Zhu, R.G., Pan, Y.Y., Guo, W., Zheng, N.J., Liu, Y.H., et al., 2020a. Differentiation between nitrate aerosol formation pathways in a Southeast Chinese city by dual isotope and modeling studies. *J. Geophys. Res.-Atmos.* 125, 13.
- Xiao, H.W., Wu, J.F., Luo, L., Liu, C., Xie, Y.J., Xiao, H.Y., 2020b. Enhanced biomass burning as a source of aerosol ammonium over cities in central China in autumn. *Environ. Pollut.* 266, 115278.
- Xie, Y.J., Lu, H.B., Yi, A.J., Zhang, Z.Y., Zheng, N.J., Fang, X.Z., et al., 2020. Characterization and source analysis of water-soluble ions in PM_{2.5} at a background site in central China. *Atmos. Res.* 239, 104881.
- Xu, L.L., Duan, F.K., He, K.B., Ma, Y.L., Zhu, L.D., Zheng, Y.X., et al., 2017. Characteristics of the secondary water-soluble ions in a typical autumn haze in Beijing. *Environ. Pollut.* 227, 296–305.
- Yang, F., Tan, J., Zhao, Q., Du, Z., He, K., Ma, Y., et al., 2011. Characteristics of PM_{2.5} speciation in representative megacities and across China. *Atmos. Chem. Phys.* 11, 5207–5219.
- Yang, H., Song, X., Zhang, Q., 2020a. Rs&Gis based PM emission inventories of dust sources over a provincial scale: a case study of Henan Province, central China. *Atmos. Environ.* 225, 117361.
- Yang, L.M., Wang, S.B., Duan, S.G., Yan, Q.S., Jiang, N., Zhang, R.Q., et al., 2020b. Characteristics and formation mechanisms of secondary inorganic ions in PM_{2.5} during winter in a central city of China: based on a high time resolution data. *Atmos. Res.* 233, 104696.
- Yang, Y.R., Liu, X.G., Qu, Y., An, J.L., Jiang, R., Zhang, Y.H., et al., 2015. Characteristics and formation mechanism of continuous hazes in China: a case study during the autumn of 2014 in the North China Plain. *Atmos. Chem. Phys.* 15, 8165–8178.
- Ye, S.Q., Ma, T., Duan, F.K., Li, H., He, K.B., Xia, J., et al., 2019. Characteristics and formation mechanisms of winter haze in Changzhou, a highly polluted industrial city in the Yangtze River Delta, China. *Environ. Pollut.* 253, 377–383.

- Zhang, R., Sun, X.S., Shi, A.J., Huang, Y.H., Yan, J., Nie, T., et al., 2018. Secondary inorganic aerosols formation during haze episodes at an urban site in Beijing, China. *Atmos. Environ.* 177, 275–282.
- Zhang, R.Y., Wang, G.H., Guo, S., Zarnora, M.L., Ying, Q., Lin, Y., et al., 2015. Formation of urban fine particulate matter. *Chem. Rev.* 115, 3803–3855.
- Zhang, Y., Cai, J., Wang, S., He, K., Zheng, M., 2017. Review of receptor-based source apportionment research of fine particulate matter and its challenges in China. *Sci. Total Environ.* 586, 917–929.
- Zhao, X.J., Zhao, P.S., Xu, J., Meng, W., Pu, W.W., Dong, F., et al., 2013. Analysis of a winter regional haze event and its formation mechanism in the North China Plain. *Atmos. Chem. Phys.* 13, 5685–5696.
- Zheng, B., Zhang, Q., Zhang, Y., He, K.B., Wang, K., Zheng, G.J., et al., 2015. Heterogeneous chemistry: a mechanism missing in current models to explain secondary inorganic aerosol formation during the january 2013 haze episode in North China. *Atmos. Chem. Phys.* 15, 2031–2049.
- Zou, J.N., Liu, Z.R., Hu, B., Huang, X.J., Wen, T.X., Ji, D.S., et al., 2018. Aerosol chemical compositions in the North China Plain and the impact on the visibility in Beijing and Tianjin. *Atmos. Res.* 201, 235–246.